Available online at www.sciencedirect.com
SCIENCE DIRECT®
International Journal of Heat and Fluid Flow 24 (2003) 825–834
International Journal of HEAT AND FLUID FLOW
www.elsevier.com/locate/ijhff

Simulations of flow through open cell metal foams using an idealized periodic cell structure

K. Boomsma, D. Poulikakos *, Y. Ventikos

Laboratory of Thermodynamics in Emerging Technologies, Swiss Federal Institute of Technology, ETH Center, ML J 36, Zürich 8092, Switzerland

Received 13 November 2002; accepted 16 August 2003

Abstract

A new approach to modeling the flow through a porous medium with a well defined structure is presented. This approach entailed modeling an idealized open cell metal foam based on a fundamental periodic unit of eight cells and solving the flow through the three-dimensional cellular unit. To model an infinitely large matrix, periodic boundary conditions were set on the walls parallel to the flow direction, while a pseudo-periodic boundary condition with a prescribed volumetric flow rate was set over the inlet–outlet pair of the unit cell. The pressure drop data of the flow through the cellular unit were then compared on a length-normalized basis against experimental data. The pressure drop values predicted by the simulations were consistently 25% lower than the values obtained in the experiments on a similar foam and under identical flow conditions. One explanation for the discrepancy between the two sets of data is the lack of pressure drop increasing wall effects in the simulations. The increase in the pressure drop from wall effects in the simulation was quantified.

Keywords: Metal foam; Porous media; Microscale approach; Numerical simulations

1. Introduction

As shown in the experimental work by Boomsma and Poulikakos (2002), Lage et al. (1996), and Bhattacharya et al. (2002), open cell metal foams perform well in forced convection heat transfer applications in addition to their wide variety of other uses such as light-weight high-strength structural applications, mechanical energy absorbers, filters, pneumatic silencers, containment matrices and burn rate enhancers for solid propellants, flow straighteners, catalytic reactors, heat sinks, and heat exchangers. Having a material with great potential for flow type applications leads to the development of a suitable model to optimize foam configurations. Modeling of porous media flows of the nature we are interested in falls under two distinct categories: macroscopic, where volume averaging is performed and microscopic, where the details of the flow in/around individual structural elements of the medium are examined.

There have been several approaches taken to model the fluid flow through porous media, both analytical and numerical. These models progressed starting with regularly packed beds of spheres, then moving to more porous fibrous media, and finally to open cell metal foams. Geometric modeling of the foam is significantly more difficult than that of packed beds of spheres due to the foam's more intricate geometry (Boomsma and Poulikakos, 2001). Despite this, many of the existing analytical and numerical models based on flow through granular media have been adapted to describe the flow through open cell metal foams, with limited success.

1.1. Previous numerical approaches

A wide variety of analytical and numerical models for porous media analysis have appeared in the literature. The first of such models is the Darcy law, which was the first mathematical model of the pressure drop (Δp) of a porous medium of a length (L) and a permeability (K) to the flow velocity (U) in a porous medium based on experimental observations:

$$\frac{\Delta p}{L} = \frac{\mu}{K} U \tag{1}$$

Dupuit's law (1863) includes a quadratic term, which is important in the higher flow velocity range:

* Corresponding author. Tel.: +41-1-632-2738; fax: +41-1-632-1176.
E-mail address: dimos.poulikakos@ethz.ch (D. Poulikakos).

0142-727X/$ - see front matter © 2003 Elsevier Inc. All rights reserved.
doi:10.1016/j.ijheatfluidflow.2003.08.002

Nomenclature

A	area [m^2]
C	form coefficient [m^{-1}]
K	permeability [m^2]
L	length [m]
PPI	pores per inch [–]
$\dot{Q}$	Volumetric flow rate
Re	Reynolds number [–]
REV	representative elementary volume [–]
$\underline{U}$	velocity [$m\,s^{-1}$]
V	three-dimensional velocity [$m\,s^{-1}$]
W	longitudinal velocity [$m\,s^{-1}$]
d	diameter [m]
$\vec{n}$	normal [–]
p	pressure [Pa]
Greeks	
Δ	change [–]
ε	porosity [%]
μ	dynamic viscosity [$kg\,m^{-1}\,s^{-1}$]
ρ	density [$kg\,m^{-3}$]
Subscripts	
K	permeability
o	specific
p	pore
target	desired value
z	axial direction

$$\frac{\Delta p}{L} = \frac{\mu}{K}U + \frac{\rho c_F}{\sqrt{K}}U^2 \tag{2}$$

The range of validity of these two models is dependent on the Reynolds number (Re) of the flow as shown by Kaviany (1995), Boomsma and Poulikakos (2002), and Antohe et al. (1997). In porous media, there are two methods of calculating the Re of a flow. The first is the permeability based method (Eq. (3)). This method is popular in the studies on granular media because the permeability is something that is relatively easily measured through experimentation:

$$Re_K = \frac{\rho U K^{1/2}}{\mu} \tag{3}$$

This method as mentioned above works well for various types of porous media, however, open cell metal foam is a special case due to its high porosity and well defined solid structure. As was seen in the work by Boomsma and Poulikakos (2002) and Antohe et al. (1997), a better method for characterizing the flow through an open cell metal foam is the pore based Reynolds number (Eq. (4)). In this method, the square root of the permeability in Eq. (3) is replaced by the average pore diameter, d_p. This approach considers the pressure drop controlling specific surface area as a function of the pore diameter:

$$Re = \frac{\rho U d_p}{\mu} \tag{4}$$

Various volume averaging approaches have been used to predict the flow and heat transfer behavior through a variety of porous media, predominantly in granular media. These types of volume averaging approaches work under the condition specified by the Re (Kaviany, 1995; Renken and Poulikakos, 1988). Good examples of models which are based on volume averaging of porous media in this fashion are those by Vafai and Tien (1981), Vafai et al. (1985), Vafai (1984), and Poulikakos and Renken (1987). However, when considering the previously made Re restriction on these models, the conditions which exist in open cell metal foams go beyond these limitations made for volume averaging models developed on packed beds of granular media. The Reynolds number in foams is often much higher than that reached in packed beds of granular media because the foam is typically much more porous ($50\% < \varepsilon < 98\%$) with a higher possible flow velocity due to the higher porosity. Plus, the form of the foam structure is quite different than that of the spheres or densely packed granular media (Fig. 1), which may cause unpredictable flow patterns to develop and alter the outcome of a model which was based on granular media.

These issues can be overcome by taking a new approach to viewing the highly porous open cell metal foam medium and attempting to directly model the geometry by defining a representative elementary volume

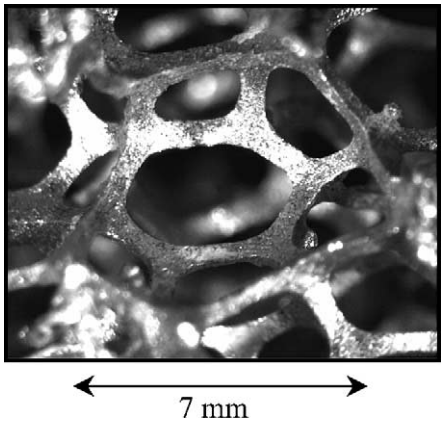

Fig. 1. A close-up of a single cell in an open cell metal foam.

(REV) that captures the intricate details of the foam structure. A similar approach was taken by du Plessis et al. (1994). In this work, they developed an REV which attempted to capture the relevant characteristics of an open cell metal foam based on a set of rectangular prisms. They used the results of an analytical flow analysis on this REV to solve the flow through an open cell foam on a larger scale with relatively good results. This investigation was later improved by Diedericks and du Plessis (1997) to include the development of a momentum transport equation that was valid in both the linear and quadratic pressure drop regimes in an open cell metal foam. From these results, it was seen that the flow through an REV could be reasonably well modeled by the flow around a system of cylinders. Lu et al. (1998) took the approach of modeling the fluid flow through open cell metal foams as a system of cylinders in their combined flow and heat convection model. Known relations for both the fluid flow and convection coefficient around a cylinder were employed to develop a numerical model valid for an entire assembly of cylinders which defined a fibrous medium. The numerical work was compared to experiments with reasonably good results, and it additionally highlighted a detailed set of heat exchanger design parameters applied to the reported numerical findings. A direct application of a numerical flow and heat convection model to open cell metal foams was performed by Lage et al. (1996). In this work they reported the results of a volume averaged numerical model used to predict the flow and heat convection of a synthetic oil flowing through a large open cell metal foam heat exchanger used to cool electronics which generated a large quantity of excess heat.

1.2. Detailed cell modeling

As seen in the work done by Smit and du Plessis (1999), Diedericks and du Plessis (1997), and du Plessis et al. (1994), the cell modeling approach simulating the flow through a porous medium has had some success, but at these coarse levels of cell representation by rectangular prisms was not precise enough to capture the required flow behavior induced by the intricate geometry of the open cell metal foam. However, with rapid advances in computing power, taking the approach of detailed cell model with a correspondingly fine volumetric mesh becomes more viable to simulate the flow through an open cell metal foam. If the individual periodic cell in an open cell metal foam consisting of a large periodic matrix is accurately modeled, the flow through the individual cell can be solved with periodic boundary conditions, thereby modeling the presence of surrounding cells with the identical flow field. By this method, the individual periodic cell is then able to capture all flow characteristics of a larger porous matrix (Koch et al., 1989).

The next step in the direct cell modeling process is recreating what is to be considered the most representative cell structure of an open cell metal foam. Because the open cell metal foams that were used in the experiments were manufactured following the DUOCEL production process, the structure of the foam takes on the shape of a foamed polymer, and not a molten metal which generates a closed cell foam that lacks an easily distinguished cell geometry (Baumeister, 1997). The polymer foam in the DUOCEL production process takes on a surface tension dominated shape. This simplifies the cell modeling process when a surface minimization program is used, such as Surface Evolver. This program was developed by Brakke (1992), and the foam model created using Surface Evolver was first presented by Phelan et al. (1996). Through the use of Surface Evolver, the numerically optimized ideal periodic shape of a foam can be modeled and later meshed for importation into a flow solver. The pressure drop from the flow simulations can be compared to the pressure drop data obtained from flow experiments that were performed on the uncompressed foam blocks as reported in Boomsma and Poulikakos (2002) as a validity check on the numerical simulations.

2. Foam structure

2.1. Cell packing

The first step in understanding the structure of a cell is obtained by considering how cells of equal volume pack themselves under pressure to most efficiently use space. This problem has been researched through various approaches. A historically popular experimental approach was the pea-packing experiment. In this experiment, peas were compressed inside a container. The resulting packed peas were then carefully observed and the number and shape of the flattened sides were recorded. From these and similar experiments Lord Kelvin postulated that the ideal packing cell shape was the so-called "tetrakaidecahedron" which is a figure consisting of six planar quadrilateral faces and eight non-planar hexagons of zero net curvature (Thomson, 1887). This shape also satisfies Plateau's conditions for a network of foam films. Surfaces which bound the cells meet at 120°, and the lines which are formed by their intersections meet at $\cos^{-1}(-1/3)$, the tetrahedral angle (Weaire and Phelan, 1994). Lord Kelvin also developed analytical expressions for the shape of the quadrilateral and hexagonal faces, and of the tetrakaidecahedron's 36 equal, planar, non-circular arcs (Weaire and Phelan, 1996) which allow the tetrakaidecahedron to completely fulfill Plateau's rules for packing cells. Fig. 2 depicts a single tetrakaidecahedron cell as described by Lord Kelvin for a foam which is essentially "dry", meaning

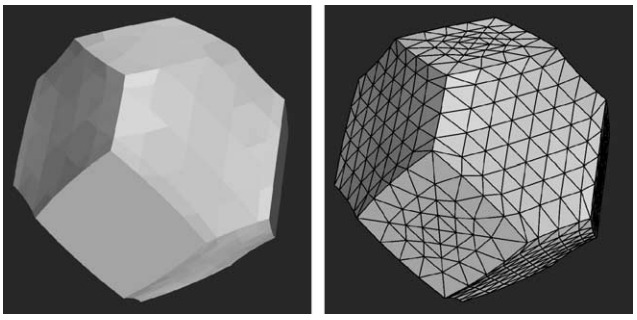

Fig. 2. The 14-sided tetrakaidecahedron cell which has long been considered the optimal packing cell first proposed by Lord Kelvin in 1887. Notice the curvature of the edges on the cell in both pictures. The cell at the right has the triangulation of the surface elements highlighted for clarity of the 3-D structure.

that the porosity is very close to 100% and the foam is basically a set of films, which is seen in reality when soap foam is observed.

The tetrakaidecahedron shape was decided upon mainly through experimentation, and has never been mathematically proven to be the optimal packing cell. With this open end, researchers have attempted to improve upon this cell through numerical methods. A successful attempt was performed by Weaire and Phelan (1994). These researchers developed a periodic unit of cells which reduced the surface energy of the packing cells by 0.3% when compared to the tetrakaidecahedron of Lord Kelvin while still holding to Plateau's rules for a periodic cellular matrix. This unit of eight equal volume cells consists of six 14-sided polyhedra having 12 pentagonal and two hexagonal faces, and two pentagonal dodecahedra. This periodic unit of optimal packing cells is shown in Fig. 3.

Adding a second phase to the foam films shown in Fig. 3 is a procedure called "wetting" which refers to increasing the fluid fraction during the foaming process. This process not only reduces the porosity of the final foam structure, but more importantly, it generates a foam that resembles the foam precursor that was used for the open cell metal foams that were tested in

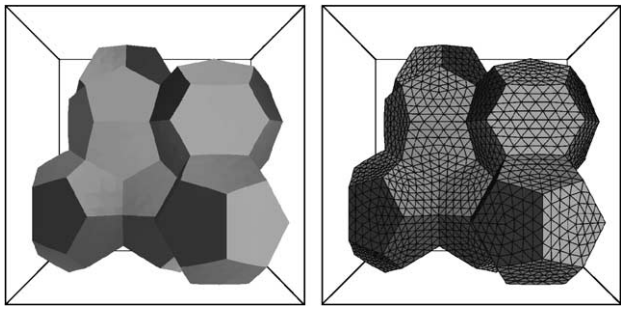

Fig. 3. The eight cell periodic unit which reduces the surface energy by a margin of 0.3% when compared to the tetrakaidecahedron Fig. 2. The figure at right shows the triangulation of the surface elements for clarity.

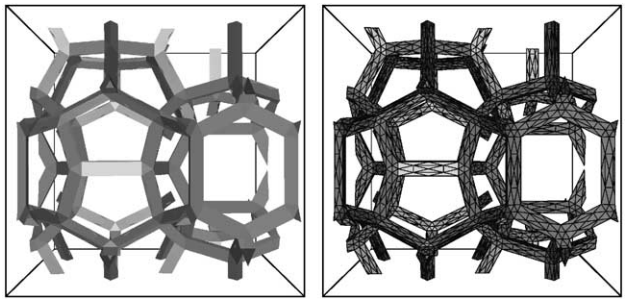

Fig. 4. The same foam structure as depicted in Fig. 3, but now the foam has been wetted and the inter-cellular membranes have been removed to model the open cell metal foam.

Boomsma and Poulikakos (2002), which had a porosity between 92% and 96%. This wetting process is easily accomplished with a foam-wetting command in Surface Evolver which can be indirectly adjusted for various surface tension values. The foam in Fig. 3 was wetted by this procedure for a final porosity of approximately 96%. The membranes between the cells were removed, and the final geometry is shown in Fig. 4. The structure and orientation of the geometry correspond to the non-wetted cells displayed in Fig. 3.

To hold to Plateau's rules for a periodic cellular structure, the second phase introduced into the foam through the wetting process must also be subjected to the same surface energy minimization process. Through this process, the Plateau borders containing the second, solid phase are created between the cells, as defined by Phelan et al. (1996). The characteristic triangular cross-section of the foams is already apparent in Fig. 4, but a close-up of the detailed intersection of the Plateau border shaped foam ligaments at the tetrahedral angle can be clearly seen in Fig. 5.

2.2. Periodic representation

The basic periodic cellular unit of the foam structure as depicted in Fig. 4 can be used as a building block to represent a much larger foam network. This is accomplished by meshing the visible void region of the structure in Fig. 4 as a fluid volume with a periodic grid at the boundaries. Proper boundary conditions are then selected so that this volume mesh becomes a representative

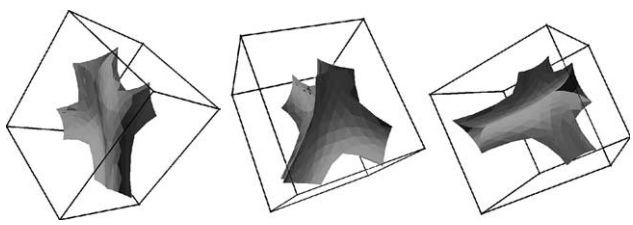

Fig. 5. This is a close-up of the tetrahedral joints of the Plateau borders that are generated by Surface Evolver when modeling a wetted foam, similar to that in Fig. 4.

elementary volume in a volume averaging technique as presented in Whitaker (1999). A longitudinal axis is selected as the primary flow direction and a periodic velocity boundary condition with a prescribed mass (volumetric) flow rate is set across the inlet–outlet boundary pair. This boundary condition models an infinitely large foam matrix in the primary velocity direction and simultaneously drives the flow. Periodic boundary conditions are set in the remaining two directions which simulate an infinitely large foam network in these directions, perpendicular to the primary flow direction.

The procedure from cell modeling to the final flow solving consists of the following steps:

1. The foam geometry is defined in an input file developed by Phelan et al. (1995) in the Surface Evolver surface energy minimization program, as described in Brakke (1992).
2. A second phase is added to the foam via the "wetfoam.cmd" command provided by Surface Evolver. The virtual surface tension and porosity of the final foam can be adjusted by changing specified parameters within the wetfoam.cmd file.
3. The wetted foam now passes through a series of elemental refinements and iterative surface energy minimization processes.
4. After numerical convergence, the resulting geometry file is exported into an ASCII file.
5. The exported geometry file is imported into the Hypermesh mesh generation program (Altair Engineering).
6. A bounding box is constructed and the foam is trimmed at the intersection with the bounding box so that the cell ligaments are fused with the bounding box.
7. A 2-D triangular mesh is generated on the surfaces of the solid cell structure and on three adjacent sides of the bounding box.
8. The triangular meshes on the bounding box surfaces are projected onto opposing sides to create identical surface meshes for periodic boundary conditions with node-to-node correspondence.
9. An unstructured 3-D tetrahedral mesh is generated within the volume defined by the connectivity of the 2-D triangular surface grids.
10. The appropriate boundary conditions are defined, along with the fluid properties and the configuration is solved, always for a pre-specified flow rate.

3. Flow solving procedure

3.1. Grid generation

The wetted foam structure seen in Fig. 4 was imported into Hypermesh to mesh the void region as the flow domain. Fig. 6 shows the 2-D surface grid on the surface of the foam structure from the first attempt of the meshing procedure on the wetted Weaire–Phelan periodic unit of 96% porosity. The REV length was chosen as one periodic length of the unit cell structure, which corresponded to two cell lengths. Adding to the REV as seen in Fig. 6 in any direction will simply build a larger foam network with adjoining solid Plateau borders. Tetrahedral elements were used to generate the first attempt of the unstructured mesh with a count of 219,656 elements and 46,199 vertices.

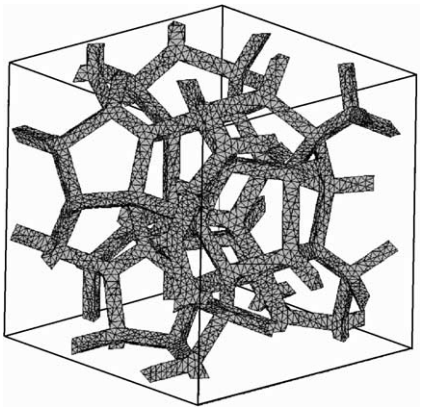

Fig. 6. The 2-D surface grid on the foam structure of a coarse unstructured mesh of the Weaire–Phelan periodic cellular unit with 219,656 tetrahedral elements and 46,199 vertices.

To check the mesh dependency of the solution, the same Weaire–Phelan structure in Fig. 6 was further refined to total 440,229 tetrahedral cells and 91,651 vertices while maintaining 96% porosity. This mesh was then further refined to 826,321 tetrahedral elements with 169,266 vertices. The pressure and velocity data from the three meshes of varying refinement were compared to determine if a mesh-independent solution was reached.

3.2. Flow solving routine

The geometry in Fig. 6 was imported into an unstructured mesh flow solver to solve the flow through the fluid domain. The unstructured flow solver chosen was CFD-ACE, which is licensed and distributed by CFDRC of Huntsville, USA. The steady, three-dimensional Navier–Stokes equations, along with conservation of mass, are solved via a control volume, pressure correction, unstructured mesh topology approach employing multi-grid acceleration. The flow through each of the grids was first solved by using an upwind scheme with an algebraic multi-grid solver and a convergence criterion of 1×10^{-8} to provide an initial condition for the central differencing scheme, which was used for a more accurate solution of the flow field in the reported results. The grids were scaled so that the average diameter of the cells corresponded to that of the 40 PPI foam that was tested in Boomsma and Poulikakos (2002) which was 2.3 mm. The volumetric flow rate of

1.587×10^{-6} m^3/s was set in the periodic boundary condition subroutine on the inlet to target an average flow velocity of 0.075 m/s. With water at 295 K as the working fluid, this volumetric flow rate corresponded to a mass flow rate of 0.001582 kg/s through the 4.6 mm $\times$ 4.6 mm $\times$ 4.6 mm cell.

The user subroutine feature of CFD-ACE allows one to prescribe custom boundary conditions. However, to apply true periodic boundary conditions over an inlet–outlet pair with a flow-driving pressure drop as was done by Patankar et al. (1977) or simply a volumetric flow rate, one would have to directly implement the connectivity between the geometrically corresponding nodes over the inlet and outlet boundaries in the solver, which was not possible with CFD-ACE. In this case a pseudo-periodic condition was developed which simulated a periodic boundary condition over the inlet–outlet pair. This was accomplished through a subroutine added to the solver which performed the following steps:

1. The faces of the inlet and outlet boundaries are assigned as periodic pairs corresponding to their geometric positions, differing only by an offset in the flow direction.
2. Zero pressure is set at the outlet and a uniform inflow velocity corresponding to the target volumetric flow rate is set at the inlet for the first iteration.
3. After the iteration, the computed three-dimensional velocity vectors at the outlet are read.
4. The axial velocity component (z-direction) is used to calculate the volumetric flow rate at the outlet according to Eq. (5):

$$\dot{Q} = (\vec{V}\cdot\vec{n}_z)A \tag{5}$$

5. This value is compared to the target volumetric flow rate, and this axial velocity component is either reduced or increased uniformly over the entire boundary so that the newly calculated volumetric flow rate equals the targeted value according to Eq. (6):

$$U_{z,\mathrm{new}} = \frac{\dot{Q}_{\mathrm{target}} - \dot{Q}}{\|\vec{A}\|} - U_{z,\mathrm{old}} \tag{6}$$

6. This 3-D velocity vector using the same x- and y-components with the newly calculated z-component $(U_x, U_y, U_{z,\mathrm{new}})$ is set at the inlet according to its corresponding boundary facial coordinate.
7. The system is iterated and the process loops back to Step 3 until convergence.

4. Results and discussion

4.1. Pressure and flow velocities

The simulation data from the three grids using a volumetric flow rate of 1.587×10^{-6} m^3/s, corresponding to an average longitudinal flow velocity of 0.075 m/s and a mass flow rate of 0.001582 kg/s with water at 295 K ($\rho = 997$ kg/m^3), were analyzed for the average flow velocity and the longitudinal velocity and pressure profiles at the inlet and outlet. The profile lines were taken through the midpoint of the periodic cellular unit, extending from one edge of the unit to the other as shown in Fig. 7. The solid line at the base of the REV crosses the flow inlet and the dashed line at the top crosses the REV outlet. The large vertical arrow shows the longitudinal flow direction.

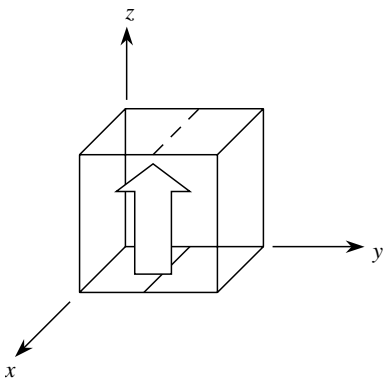

Fig. 7. A diagram of where the pressure and longitudinal velocity profiles were taken to measure the accuracy of the pseudo-periodic boundary condition over the inlet–outlet boundary pair.

Fig. 8 depicts the pressure difference and velocity profiles over the simulated periodic inlet–outlet pair for the flow speed of 0.075 m/s. This figure shows simultaneously an estimate of the pressure drop associated with the specified volumetric flow rate (1.5870×10^{-6} m^3/s) and the accuracy of the user-defined periodic flow boundary condition using a specified volumetric flow rate. The spike seen in the pressure difference profile of Fig. 8 is a result of the coarse mesh used at the boundary between the edge of the periodic cellular unit and the solid phase of the system. Figs. 9 and 10 show the same plots for the two refined meshes.

Comparing the accuracy of the periodicity of the pressure and longitudinal velocity profiles from the three different meshes revealed the effectiveness of the user-defined periodic boundary condition when applied to an inlet–outlet pair. Ideally the pressure difference profile between the inlet and outlet should be a straight line at the value of the pressure drop over the cell. However, in the user subroutine implemented to define the periodic inlet–outlet condition, only the 3-D velocity vector was set at the inlet, thereby allowing the pressure to freely adjust itself to the flow conditions. The longitudinal velocity profiles over the inlet–outlet pair nearly overlap with the rough mesh (Fig. 8), and become closer to each other with the first mesh refinement (Fig. 9), until they ultimately fall onto the same curve with the highly refined mesh (Fig. 10). These profiles overall showed that

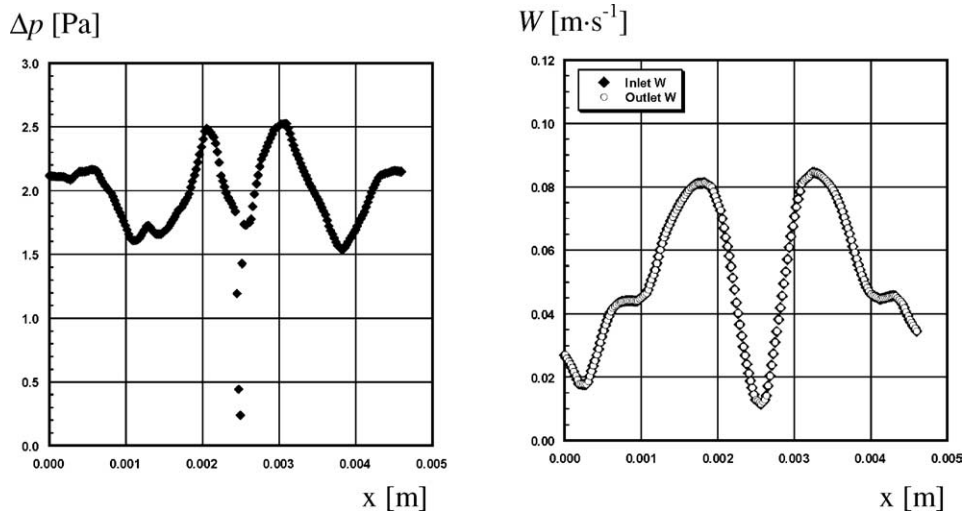

Fig. 8. Pressure drop and axial velocity profiles of the coarse mesh (219,656 tetrahedral elements) generated with a central solving scheme over the periodic inlet–outlet pair.

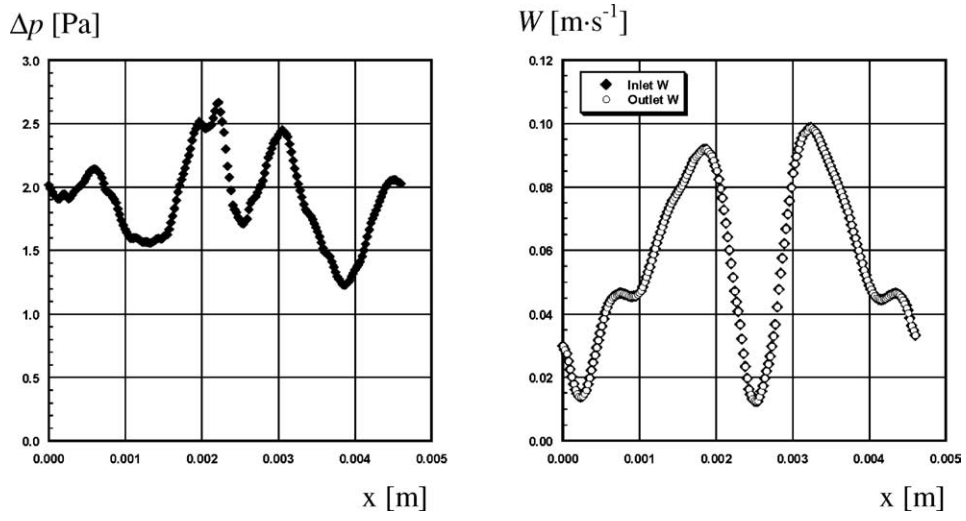

Fig. 9. Pressure drop and axial velocity profiles of the first refined mesh (440,229 tetrahedral elements) generated with a central solving scheme over the periodic inlet–outlet pair.

the user subroutine which prescribes a volumetric flow rate and sets the inlet velocity from the outlet velocity data with a longitudinal velocity correction is a reasonable approach to generating the velocity component of a periodic inlet–outlet boundary condition. Fig. 11 illustrates some of the flow characteristics observed in this REV, though the depiction of a selection of characteristic streamlines.

4.2. Comparison to experiments

The pressure drop results from the numerical simulations differing only by the level of mesh refinement were compared to the pressure drop results of the experiments that were reported in Boomsma and Poulikakos (2002) which most closely modeled both the foam form and flow conditions. The meshes of the numerical simulations were scaled so that the average pore diameter was 2.3 mm, which corresponded to the 40 PPI foam that was tested in Boomsma and Poulikakos (2002). In the experiment, water was used with a bulk velocity of 0.075 m/s, passing through an open cell metal foam of 92% porosity and overall dimensions of 12.0 mm × 38.0 mm × 80.0 mm long. The pressure results obtained by averaging the 2-D pressure profiles on the inlet and outlet boundaries from the three different meshes are tabulated in Table 1.

The porosity of the foam in the simulations was 96%, compared to the porosity of the foams tested in Boomsma and Poulikakos (2002) which was 92%. This

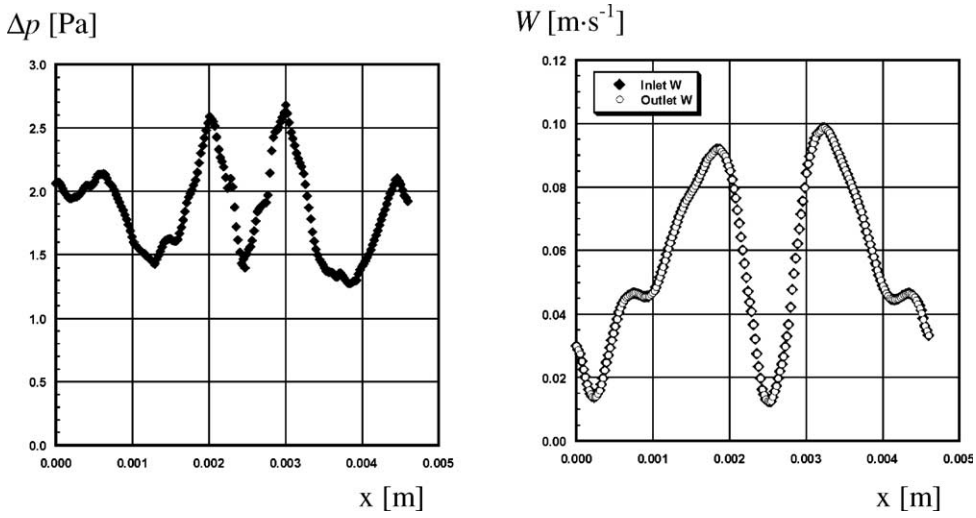

Fig. 10. Pressure drop and axial velocity profiles of the highly refined mesh (826,321 tetrahedral elements) generated with a central solving scheme over the periodic inlet–outlet pair.

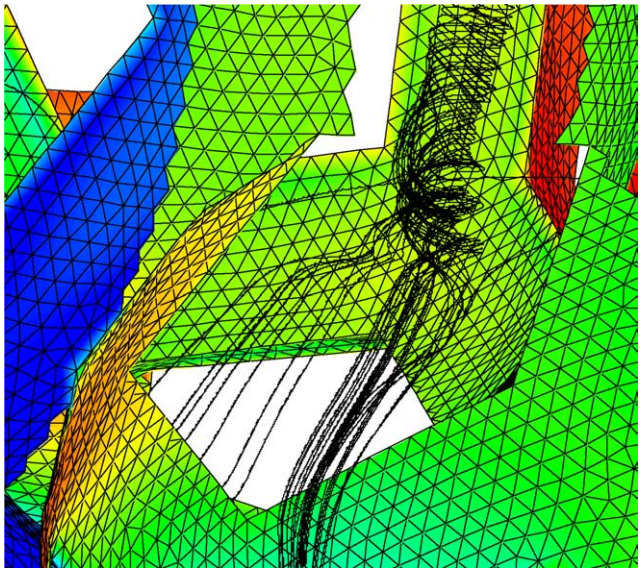

Fig. 11. Selection of representative streamlines depicting features of the flow through the REV: surface pressure distribution and formation of a three-dimensional recirculation region behind one of the foam ligaments.

difference in porosity makes little difference in the experimental comparison. In the experimental work by Bhattacharya et al. (2002), for open cell foams with pore diameters of approximately 2 mm within a porosity range between 91% and 96%, the overall flow resistance remained nearly constant. This shows the pore diameter, and not the porosity, increases the specific surface area (A_o) through the geometrical relationship involved in the scaling of the structure as confirmed by Boomsma and Poulikakos (2002). This increase in the specific surface area has a larger effect on the permeability and overall flow resistance of a foam than an increase in the solid fraction of the foam, since viscous drag is the dominating factor of pressure drop through a porous medium (Lage, 1998), which is governed by the solid-fluid interfacial area. With this knowledge, the pressure drop information from the numerical simulations which were done on a mesh scaled to that of the 40 PPI open cell metal foam (2.3 mm pore diameter) can be directly compared to the results of the pressure drop experiments done on the 92% porous foam without extrapolating.

The pressure drop varied up to 7% between the grids of varying refinement, but the pressure drop obtained from the simulations remained within 1% between the two refined meshes, validating the mesh-independent results from these simulations. The length-normalized pressure drop obtained from the simulations was approximately 25% lower than the pressure drop from the experiment performed on a similar foam. One explana-

Table 1
Comparison of the measured pressure drop with the computed one, for the various grids

Mesh #	Mesh description		Simulation Dp		Experimental Dp	Difference (%)
	Cells	Vertices	Measured [Pa]	Normalized [bar/m]	Normalized [bar/m]	
1	219,656	46,199	9.0	0.0197	0.0270	−27.2
2	440,229	91,651	9.5	0.0206	0.0270	−23.8
3	826,321	169,266	9.6	0.0209	0.0270	−22.7

tion is the lack of wall effects in the simulation which were, however, present in the experiment (Mehta and Hawley, 1969). To determine the effects of the foam container walls on the overall pressure drop of the flow through the foam, numerical simulations were carried out on Mesh #3 with substituting no-slip walls for the periodic boundaries parallel to the flow. As expected, the overall pressure drop for the same flow velocity of 0.075 m/s did increase significantly in the tightly walled periodic cellular unit, reaching a value of 0.0303 bar/m, something that has been observed in other studies too, Vafai and Tien (1981). This pressure drop value exceeds the experimental pressure drop value from the flow through the foam of the same pore diameter by 12%, thereby confirming the periodic walls as the cause of the discrepancy between the pressure drop values obtained in the simulations.

5. Conclusion

A new approach for modeling the flow through an intricately structured porous medium was presented. This method emulates a periodic boundary condition over the inlet–outlet pair, driving the flow by specifying a volumetric flow rate and adjusting the velocity distribution at the inlet according to the flow velocity at the outlet. The mesh-independent results from the numerical simulations on the flow through the foam were compared to experiments with good agreement, considering the increased flow resistance generated by wall effects from the foam container in the experiment on the pressure drop. This pressure drop increase by the container walls was also demonstrated in numerical simulations where no-slip container walls substituted the periodic boundaries containing the flow.

Acknowledgements

It is gratefully acknowledged that this research was supported jointly by the Swiss Commission for Technology and Innovation (CTI) through project no. 4150.2 and by the ABB Corporate Research Center, Baden–Dättwil, Switzerland. CFD-RC (Huntsville AL) is kindly acknowledged for the use of the CFD-ACE software platform.

References

Antohe, B.V., Lage, J.L., Price, D.C., et al., 1997. Experimental determination of permeability and inertia coefficients of mechanically compressed aluminum porous matrices. Journal of Fluids Engineering—Transactions of the ASME 119, 404–412.

Baumeister, J. 1997. Überblick: Verfahren zur Herstellung von Metallschäumen. In: Symposium Metallschäume, Bremen, Germany, Metall Innovation Technologie (MIT).

Bhattacharya, A., Calmidi, V.V., Mahajan, R.L., 2002. Thermophysical properties of high porosity metal foams. International Journal of Heat and Mass Transfer 45, 1017–1031.

Boomsma, K., Poulikakos, D., 2001. On the effective thermal conductivity of a three dimensionally structured fluid-saturated metal foam. International Journal of Heat and Mass Transfer 44, 827–836.

Boomsma, K., Poulikakos, D., 2002. The effects of compression and pore size variations on the liquid flow characteristics of metal foams. Journal of Fluids Engineering—Transactions of the ASME 124, 263–272.

Brakke, K., 1992. The Surface Evolver. Experimental Mathematics 1, 141–165.

Diedericks, G.P.J., du Plessis, J.P., 1997. Modelling of flow through homogeneous foams. Mathematical Engineering in Industry 6, 133–154.

du Plessis, P., Montillet, A., Comiti, J., et al., 1994. Pressure-drop prediction for flow-through high-porosity metallic foams. Chemical Engineering Science 49, 3545–3553.

Dupuit, J., 1863. Etudes Theoriques et Pratiques sur le Mouvement des Eaux. Dunod, Paris.

Kaviany, M., 1995. Principles of Heat Transfer in Porous Media. Springer-Verlag, New York.

Koch, D.L., Cox, R.G., Brenner, H., et al., 1989. The effect of order on dispersion in porous-media. Journal of Fluid Mechanics 200, 173–188.

Lage, J.L., 1998. The fundamental theory of flow through permeable media from darcy to turbulence. In: Ingham, D.B., Pop, I. (Eds.), Transport Phenomena in Porous Media. Elsevier Science, Oxford, pp. 1–30.

Lage, J.L., Weinert, A.K., Price, D.C., et al., 1996. Numerical study of a low permeability microporous heat sink for cooling phased-array radar systems. International Journal of Heat and Mass Transfer 39, 3633–3647.

Lu, T.J., Stone, H.A., Ashby, M.F., 1998. Heat transfer in open-cell metal foams. Acta Materialia 46, 3619–3635.

Mehta, D., Hawley, M.C., 1969. Wall effect in packed columns. Industrial & Engineering Chemistry Process Design and Development 8, 280–282.

Patankar, S.V., Liu, C.H., Sparrow, E.M., 1977. Fully developed flow and heat transfer in ducts having streamwise-periodic variations of cross-sectional area. Journal of Heat Transfer—Transactions of the ASME 99, 180–186.

Phelan, R., Weaire, D., Brakke, K., 1995. Computation of equilibrium foam structures using the Surface Evolver. Experimental Mathematics 4, 181–192.

Phelan, R., Weaire, D., Peters, E.A.J.F., et al., 1996. The conductivity of a foam. Journal of Physics: Condensed Matter 8, L475–L482.

Poulikakos, D., Renken, K., 1987. Forced-convection in a channel filled with porous-medium, including the effects of flow inertia, variable porosity, and Brinkman friction. Journal of Heat Transfer—Transactions of the ASME 109, 880–888.

Renken, K.J., Poulikakos, D., 1988. Experiment and analysis of forced convective heat-transport in a packed-bed of spheres. International Journal of Heat and Mass Transfer 31, 1399–1408.

Smit, G.J.F., du Plessis, J.P., 1999. Modelling of non-Newtonian purely viscous flow through isotropic high porosity synthetic foams. Chemical Engineering Science 54, 645–654.

Thomson, W., 1887. On the division of space with minimum partitional area. Philosophical Magazine 5, 503–514.

Vafai, K., 1984. Convective flow and heat transfer in variable porosity media. Journal of Fluid Mechanics 147, 233–259.

Vafai, K., Tien, C.L., 1981. Boundary and inertial effects on flow and heat transfer in porous media. International Journal of Heat and Mass Transfer 24, 195–203.

Vafai, K., Alkire, R.L., Tien, C.L., 1985. An experimental investigation of heat transfer in variable porosity media. Journal of Heat Transfer—Transactions of the ASME 107, 642–647.

Weaire, D., Phelan, R., 1994. A counter-example to Kelvin's conjecture on minimal surfaces. Philosophical Magazine Letters 69, 107–110.

Weaire, D., Phelan, R., 1996. The physics of foam. Journal of Physics: Condensed Matter 8, 9519–9524.

Whitaker, S., 1999. The Method of Volume Averaging. Kluwer Academic Publishers, Dordrecht, The Netherlands.